TU Delft

Delft University of Technology

Hydrogenated Boron Phosphide with the excellent tunability of electronic properties and Current-Voltage responses

Tan, Chunjian; Zhou, Quan; Liu, Xu; Zhang, Guoqi ; Ye, Huaiyu; Wu, Qibao

DOI
10.1016/j.apsusc.2021.151196

Publication date
2022

Document Version
Final published version

Published in
Applied Surface Science

Citation (APA)
Tan, C., Zhou, Q., Liu, X., Zhang, G., Ye, H., & Wu, Q. (2022). Hydrogenated Boron Phosphide with the excellent tunability of electronic properties and Current-Voltage responses. *Applied Surface Science*, *572*, Article 151196. https://doi.org/10.1016/j.apsusc.2021.151196

Important note
To cite this publication, please use the final published version (if applicable).
Please check the document version above.

Copyright
Other than for strictly personal use, it is not permitted to download, forward or distribute the text or part of it, without the consent of the author(s) and/or copyright holder(s), unless the work is under an open content license such as Creative Commons.

Takedown policy
Please contact us and provide details if you believe this document breaches copyrights.
We will remove access to the work immediately and investigate your claim.

This work is downloaded from Delft University of Technology.
For technical reasons the number of authors shown on this cover page is limited to a maximum of 10.

Green Open Access added to TU Delft Institutional Repository

'You share, we take care!' - Taverne project

https://www.openaccess.nl/en/you-share-we-take-care

Otherwise as indicated in the copyright section: the publisher is the copyright holder of this work and the author uses the Dutch legislation to make this work public.

Applied Surface Science 572 (2022) 151196

Contents lists available at ScienceDirect

Applied Surface Science

journal homepage: www.elsevier.com/locate/apsusc

Full Length Article

Hydrogenated boron phosphide with the excellent tunability of electronic properties and Current-Voltage responses

Chunjian Tan [a,b,1], Quan Zhou [d,1], Xu Liu [a,b], Guoqi Zhang [a], Huaiyu Ye [b,d,*], Qibao Wu [c,*]

[a] Electronic Components, Technology and Materials, Delft University of Technology, 2628 CD Delft, the Netherlands
[b] Engineering Research Center of Integrated Circuits for Next-Generation Communications, Ministry of Education, School of Microelectronics, Southern University of Science and Technology, Shenzhen 518055, China
[c] School of Intelligent Manufacturing and Equipment, Shenzhen Institute of Information Technology, Shenzhen 518172, China
[d] University and College of Optoelectronic Engineering, Chongqing University, Chongqing 400044, China

ARTICLE INFO

Keywords:
First principles calculations
NEGF
Hydrogenation
Boron phosphide
External stimulus
Transport feature

ABSTRACT

Combining the first principles calculations and the non-equilibrium Green's function formalisms, we decipher the structural, electronic, and transport properties of boron phosphide (BP) with hydrogenation. Hydrogenated BP monolayer is an indirect semiconductor with a wide-bandgap of 3.76 eV that is favorable in power devices. We find that the electronic properties are dependent of the stacking orders and the binding strength of the AA-, AB-, and AE-stacked patterns are strongest in the investigated configurations. Under the external E-field, the bandgaps of hydrogenated BP bilayer show a quasi-parabolic function and a feature of the semiconductor-metallic transition. Besides, when we apply a tensile strain on hydrogenated BP bilayer, its bandgap linearly decreases with the increasing of the strain strength along the zigzag and armchair directions. The strain energies further confirm that hydrogenated BP has an excellent characteristic of elastic deformation, being independent of the stacking orders and strain orientation. The transport calculations exhibit various responses to the different two-probe configurations, which indicates that hydrogenated BP possesses the feature of transmission anisotropy. Owing to the nontrivial tunability and transport feature, the hydrogenated BP materials may have tremendous prospects to be applied in micro-/nano-devices with high consumption.

1. Introduction

Owing to the fast development of semiconductor technologies, the Moore's law has obtained considerable progress in recent decades. Nevertheless, its industrial influence and authority are gradually descending due to the physical limits of transistors and bulk materials. [1] In order to overcome this technical obstacle, unremitting endeavor has been still performed to research for novel FETs with smaller the feature size and higher operation performance.[2–4] The FinFETs proposed by Chenming Hu[3] broken the development dilemma of Moore's law, which possesses the smaller feature size compared with that of conventional transistors.[5] The novel device architectures enable the FinFETs to provide excellent electrostatic control capability and mitigate the short channel effect,[5,6] being considered to be the next-generation semiconductor craftwork. However, the conventional bulk materials as the channel materials of FinFETs have been unable to meet the high performance requirements due to the prominent short channel effect, thus the exploration of new channel materials is the core issue of FinFETs process. Currently, the III-V compound semiconductors have attracted much research attention as channel materials of FinFETs because they possess many advantages compared to conventional silicon based materials, such as high carrier mobility, sizeable bandgap, and lower in-plane dielectric constant, etc.[7–10]

Monolayer boron-phosphide (BP), a graphene-like III-V binary compound, is an n-type 2D crystal with the planar honeycomb structure. [11–13] It has aroused enormous interest in the field of future nanoelectronics due to the outstanding properties such as good thermoelectricity, direct-bandgap, and extraordinary mechanical characteristics, etc.[11,14–17] Although BP monolayer has not been synthesized on the experimental level, researchers have accurately predicted that its dynamic stability is stronger than that of silicene on the theoretical level. [11] Interestingly, the hole and electron mobility of BP monolayer are

* Corresponding authors.
E-mail addresses: yehy@sustech.edu.cn (H. Ye), wuqb@sziit.edu.cn (Q. Wu).
[1] ‡ These authors contributed equally to this work.

https://doi.org/10.1016/j.apsusc.2021.151196
Received 12 January 2021; Received in revised form 28 August 2021; Accepted 4 September 2021
Available online 7 September 2021
0169-4332/© 2021 Published by Elsevier B.V.

similar to those of graphene,[18] but much larger than phosphorene and BN nanosheets,[10,19,20] which may make it a very promising channel material in the field of FinFETs. Unfortunately, the small direct-bandgap of BP monolayer may become a deathful defect for the downscaling of the feature size because of the low breakdown voltage of narrow bandgap materials. The one order of magnitude larger breakdown voltage strength of materials enables a reduction of device size to 1/10 of that required for silicon.[21,22] Therefore, the tunability of BP monolayer is urgently expected to be investigated in order to meet the requirements of operation performance and feature size of FinFETs. Nowadays, hydrogenation engineering has become a powerful tool in effectively modulate the energy bandgap and the properties in the 2D materials domain.[23–25] By means of surface hydrogenation, a considerable bandgap is opened in the band structures of graphene, germanene, and silicene.[26–28] On the other hand, many previous studies have shown that the interior factors (the stacking order and hole/electron-doping) and the external perturbations (E-field and mechanical stimuli) have remarkably influence on the characteristics of 2D materials and the operation performance of nanoelectronic devices.[12,23,29] Accordingly, the surface hydrogenation of BP monolayer and the variation tendency of the corresponding properties under different conditions are worth investigating to offer practical guidance for the fundamental investigation and industrial applications.

In this article, we theoretically predict hydrogenated BP monolayer and systematically explore the influence of the interior factors and the external perturbations on the structural, electronic, and current–voltage (I-V) characteristics of hydrogenated BP monolayer from the atomic and device scale by means of the non-equilibrium Green's function (NEGF) method combined with the first-principles calculations. The phonon calculations demonstrate that hydrogenated BP monolayer has outstanding stability. The band structures show that when BP monolayer is fully hydrogenated on the surface, its bandgap is enlarged to 3.759 eV which is an indirect-gap, suggesting that hydrogenated BP monolayer possesses the high breakdown voltage. Meanwhile, the calculation results reveal that the electronic properties of hydrogenated BP monolayer can be effectively tailored by applying the stacking order, E-field, and mechanical strain. However, the I-V characteristics demonstrate that the mechanical strain and electron-doping within the certain range have almost no influence on the macroscopic properties of hydrogenated BP monolayer.

2. Computational methods

For our research, we perform the DFT calculations within the framework of three DFT implementations, namely, the Cambridge Sequential Total Energy Package (CASTEP), the DMol^3 package, and the Atomistix Toolkit (ATK) package.[30,31] The CASTEP is utilized to compute the phonon spectrum to describe the dynamical stability of BP layer with hydrogenation. The structural and electronic properties of hydrogenated BP under different conditions are discussed by adopting DMol^3 code. For ATK package, it is used to explore the transport properties with/without hydrogenation. These three DFT codes adopt the generalized gradient approximation of Perdew-Burke-Ernzerhof (GGA-PBE) as the exchange–correlation functional.[31] In order to minimize artificial interactions between two adjacent images, the vacuum thickness in the direction perpendicular to the slab surface is larger than 15 Å for all computational configurations. Additionally, a primitive cell of hydrogenated BP monolayer is used for the phonon dispersion and electronic properties calculations.

CASTEP details: The phonon dispersion is calculated by using the plane-wave basis set with Norm conserving pseudopotentials. To overcome the underestimation problem of GGA-PBE in the bandgap, the HSE06 hybrid functional method is adopted to calculate the bandgap.[32] The energy cutoff of the plane waves is set to 550 eV with the energy precision of 10^{-5} eV per atom.[33] The Brillouin zone (BZ) integrations are carried on by using a $9 \times 9 \times 1$ Monkhorst-Pack grid.

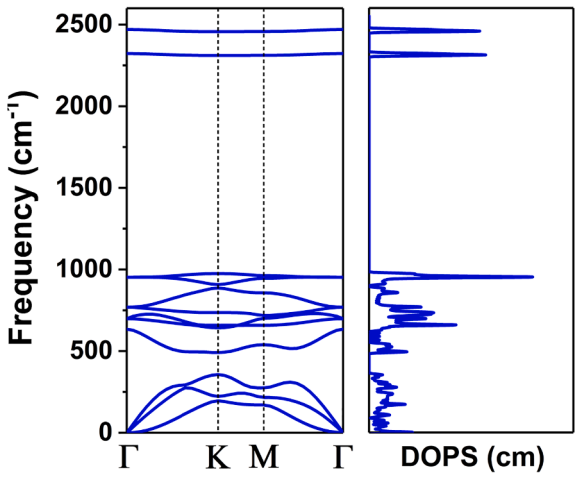

Fig. 1. Phonon frequency dispersions of hydrogenated BP monolayer.

DMol^3 details: The all-electron double numerical atomic orbital plus polarization (DNP) basis set is employed, which can effectively and accurately obtain the electronic properties and crystallographic structure. The DFT + D method within the Grimme scheme is adopted to better understand the long-range van der Waals (vdW) interaction between the neighboring layers.[23] All of atoms in the hexagonal lattice are completely relaxed by the conjugate gradient method until the residual force is less than 0.005 eV Å^{-1} and the energy convergence tolerance is set to 10^{-5} eV. The BZ is sampled by using a $24 \times 24 \times 1$ k-point within the Monkhorst-Pack scheme for geometric optimization and electronic structure computations.

ATK details: In the NEFG-DFT calculations, we adopt the double-ζ plus polarization basis set (DZP) to expand the wave functions and the Troullier-Martins pseudopotentials are used for the atomic cores.[30] The density mesh cutoff is set to 75 Hartree (1 Ha = 27.2114 eV) which meets the balance between computation efficiency and accuracy. The k-point grids of $5 \times 5 \times 100$ and 8×8 are used to sample the BZ of devices in the $\times$, y, and z direction for the self-consistent and for the I-V response and transmission spectrum, respectively. According to the Landauer – Büttiker formalism, when a finite bias voltage is applied, the current is driven to flow through the system, obtained from integration of the transmission spectrum:[34]

$$I = \frac{2e}{h}\int T(E, V_b, N_e)[f(E-\mu_L) - f(E-\mu_R)]dE$$

where $T(E, V_b)$ is the transmission probability of electrons incident at an energy E from the left to the right electrode under an applied bias voltage V_b, and $f(E-\mu_{L,R})$ is the Fermi-Dirac distribution of electrons in the left (L) and right (R) electrode with the respective chemical potential $\mu_L = E_F + V_b/2$ and $\mu_R = E_F - V_b/2$ shifted correspondingly up or down relative to the Fermi energy E_F.

3. Results and discussion

Before starting the investigation of geometric structure and electronic properties of hydrogenated BP monolayer, the authoritative evidence determining the dynamical stability of hydrogenated BP monolayer must be clarified. Consequently, the phonon spectrum along the high symmetry directions in the Brillouin zone and the density of phonon states (DOPS) of hydrogenated BP monolayer are calculated and shown in Fig. 1. The imaginary frequency is absent in the entire Brillouin zone, indicating that hydrogenated BP monolayer is kinetically stable. This is in accordance with the result obtained by Keyan *et al.*[32] In particular, the highest frequency of hydrogenated BP monolayer reaches up to 2470 cm^{-1} which is larger than that of 1600 cm^{-1} in graphane

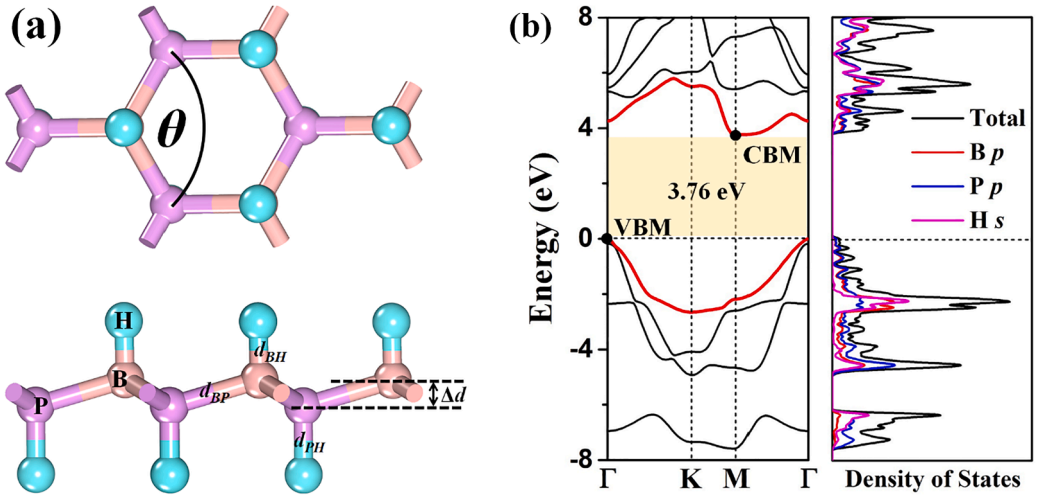

Fig. 2. (a) Top and side view of optimized geometry and (b) the band structures and partial density of states of hydrogenated BP monolayer. The Fermi level is assigned at energy zero.

Table 1
Equilibrium lattice constant (a), the length of B-P bonds (d_{BP}), the length of B-/P-H bonds (d_{BH}/d_{PH}), the buckling distance (Δd), the bond angle (θ), and band gap (ΔE) of pristine and hydrogenated BP monolayer.

Material	a (Å)	d_{BP} (Å)	d_{BH} (Å)	d_{PH} (Å)	Δd (Å)	θ (deg)	ΔE (eV)
Pristine BP	3.22	1.86	–	–	0.00	120.0	0.95 GGA 1.37 HSE06
HBPH	3.25	1.95	1.21	1.42	0.56	112.5	3.76 GGA 4.41 HSE06

[35], 2100 cm^{-1} in silicane[36], 2000 cm^{-1} in germanane[36], and 740 cm^{-1} in hydrogenated arsenene[37], whereas it is smaller than that of 3200 cm^{-1} in hydrogenated BN monolayer[38]. Therefore, the B-H and P-H bonds are more robust than C-H, Si-H, and Ge-H bonds, but weaker than B-H and N-H bonds of hydrogenated BN monolayer. In addition, the DOPS of hydrogenated BP monolayer is compatible with the phonon dispersions. The phonon results indicate that the possibility of experimental preparation of hydrogenated BP monolayer in future through the several methods.[39–41]

To achieve a rational understanding for hydrogenated BP monolayer, we first analyze the atomic structure of optimized BP monolayer bonding with H atoms, as illustrated in Fig. 2(a). The structure parameters of pristine and hydrogenated BP monolayer including the lattice constant (a), the length of B-P bonds (d_{BP}), the length of B-/P-H bonds (d_{BH}/d_{PH}), the buckling distance (Δd), and the bond angle (θ), are listed in Table 1. It should be noticed that the lattice constant after hydrogenation is 3.25 Å which is almost unchanged compared with that (3.22 Å) of pristine BP monolayer, and the corresponding B-P bond length slightly increases to 1.95 Å from 1.86 Å. Simultaneously, the lengths of B-H bond and P-H bond are 1.21 Å and 1.42 Å, being in agreement with that in hydrogenated h-BN and hydrogenated blue phosphorene, respectively.[42,43] Owing to the difference in atomic radius between B atom and P atom, the length of P-H bond is larger than that of B-H bond. The P-B-P bond angles decrease by 7.5° when H atoms are anchored on the top site of B and P atoms. In addition, hydrogenated BP monolayer possesses a buckled honeycomb structure with a buckling height of 0.56

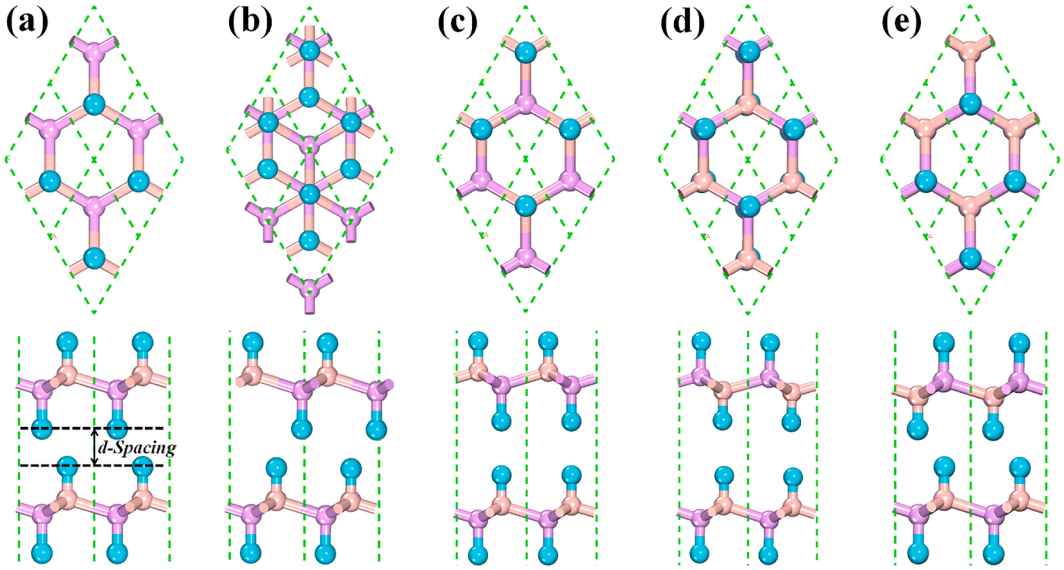

Fig. 3. Five stacking configurations of bilayer hydrogenated BP. Top and side views of the atomic structure of (a) AA-, (b) AB-, (c) AC-, (d) AD-, and (d) AE-stacking with the full relaxation.

Table 2
Relaxed lattice constants (a_h), bond lengths (d_{hBP}, d_{hBH}, and d_{hPH}), interlayer distances (d-Spacing), binding energies (E_b), and bandgaps (ΔE_h) of bilayer hydrogenated BP with five different stacking orders.

Stacking order	a_h	d_{hBP}	d_{hBH}	d_{hPH}	*d-Spacing*	E_b	ΔE_h
AA	3.227	1.946	1.212	1.420	1.413	−0.127	2.72
AB	3.227	1.946	1.212	1.420	1.485	−0.120	2.70
AC	3.227	1.947	1.212	1.422	2.157	−0.089	2.76
AD	3.236	1.952	1.211	1.424	2.251	−0.082	3.81
AE	3.225	1.945	1.208	1.423	1.407	−0.124	3.82

The units of distance and energy are Å and eV, respectively.

Å, which is caused by the sp^3 hybridization of B and P atoms.[44,45] The band structures distinctly show that hydrogenated BP monolayer is a wide-bandgap semiconductor with an indirect ΔE of 3.76 eV, where the conduction band minimum (CBM) and valence band maximum (VBM) are located at the M point and Γ point in the BZ, respectively. It indicates that hydrogenation can trigger a direct-to-indirect gap transition, where the prominent change in the effective masses could be found at the zone boundaries of the gap transition.[46,47] Furthermore, the *s* orbital of H atom is strongly hybridized with the *p* orbital of B and P atoms in hydrogenated BP monolayer, which has a prominent contribution to the DOS in the valence band and conduction band, as shown in Fig. 2(b).

Stacking order is emerging as a versatile tool to tailor the atomic structures and physicochemical properties of 2D materials, opening up numerous possibilities for shaping the future of 2D materials-based nanoelectronic and optoelectronic devices.[48–50] Moreover, as the thinnest multilayer structure in 2D materials, bilayer system can characterize the stacking-dependent electronic/optical properties and interaction between adjacent layers.[49] Consequently, it is interesting to decipher how the electronic properties of bilayer hydrogenated BP response to different stacking orders. Five possible stacking configurations of bilayer hydrogenated BP are considered, namely, AA-, AB-, AC-, AD-, and AE-stacking. As depicted in Fig. 3(a), two hydrogenated BP monolayers are directly stacked to construct the AA-stacking conformation with a perfect match in the *xy*-plane, whereas in AB-stacking (see Fig. 3(b)) the P atom of the top layer is vertically directed at the center of the benzene-like ring of the bottom layer. For the AC-stacking, it can be viewed as rotating the top layer of the AA-stacking by 180° around *z* axis perpendicular to the *xy*-plane. Subsequently, by mean of rolling-over the top layer of the AC-stacking on the vertical dimension can obtain the AE-stacking, as displayed in Fig. 3(d). In the AD-stacking, it can be noted that the top layer is a mirror image of the bottom layer. The calculated structural and electronic parameters are listed in Table 2. It is found that the lattice constants (a_h) and bond lengths (d_{hBP}, d_{hBH}, and d_{hPH}) are almost unchanged, which indicates that the structural parameters of bilayer hydrogenated BP are independent of the stacking orders. Among the five stacking configurations, the most noticeable difference is the interlayer distance (*d-Spacing*) between top and bottom layer, which varies from 1.407 Å in the AE-stacking to 2.251 Å in the AD-stacking. On the basis of the binding energies, the AA-, AB-, and AE-stacking are energetically the most favorable, their E_b are 0.038 (0.045), 0.031 (0.038), and 0.035 (0.042) eV lower than that of AC-stacking (AD-stacking). The interaction strength of layer-to-layer is stronger than that between BP layer and substrate.[47]

The band structures of AA-, AB-, AC-, AD, and AE-stacked bilayer hydrogenated BP are presented in Fig. 4(a)-(e). Surprisingly, the indirect bandgap feature is retained, where the CBM and VBM are still located at the M and Γ point.[49] This indicates that the indirect-gap feature is not sensitive to the stacking orders. It can be found that the ΔE_h of AD- and AE-stacked configurations are 0.05 and 0.06 eV higher than the ΔE of hydrogenated BP monolayer, respectively. In contract, AA-, AB-, and AC-stacked conformations show a decrease behavior in the ΔE_h values. The ΔE_h are reduced by 1.04, 1.06, and 1.00 eV when two hydrogenated BP monolayers are stacked to form AA-, AB-, AC-stacking, respectively. Therefore, stacking orders could be a powerful tool in the bandgap engineering of 2D materials. In order to gain further insights into the band structures of five stacked conformations, the corresponding isosurfaces of charge densities at CBM and VBM are depicted in Fig. 4(f)-(j). One can see that the CBMs of AA-, AB-, and AC-stacked patterns are completely localized in the top layer and contributed by the B-P bonds, representing a σ bond feature. However, their VBMs are contributed from the

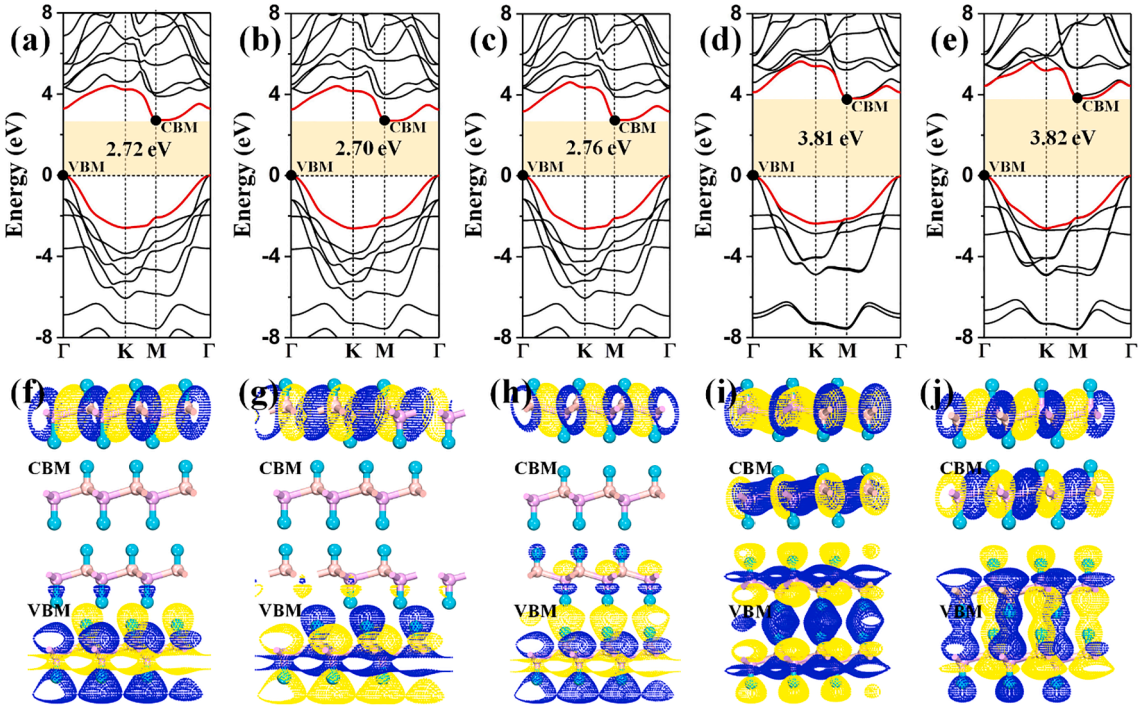

Fig. 4. Calculated band structures of (a) AA-, (b) AB-, (c) AC-, (d) AD-, and (e) AE-stacked configurations and (f, g, h, i, j) the isosurface plot of charge density corresponding to CBM and VBM of AA-, AB-, AC-, AD-, and AE-stacking. The isovalue is taken as 0.03 e/Å^3. The Fermi level is set to be 0 eV.

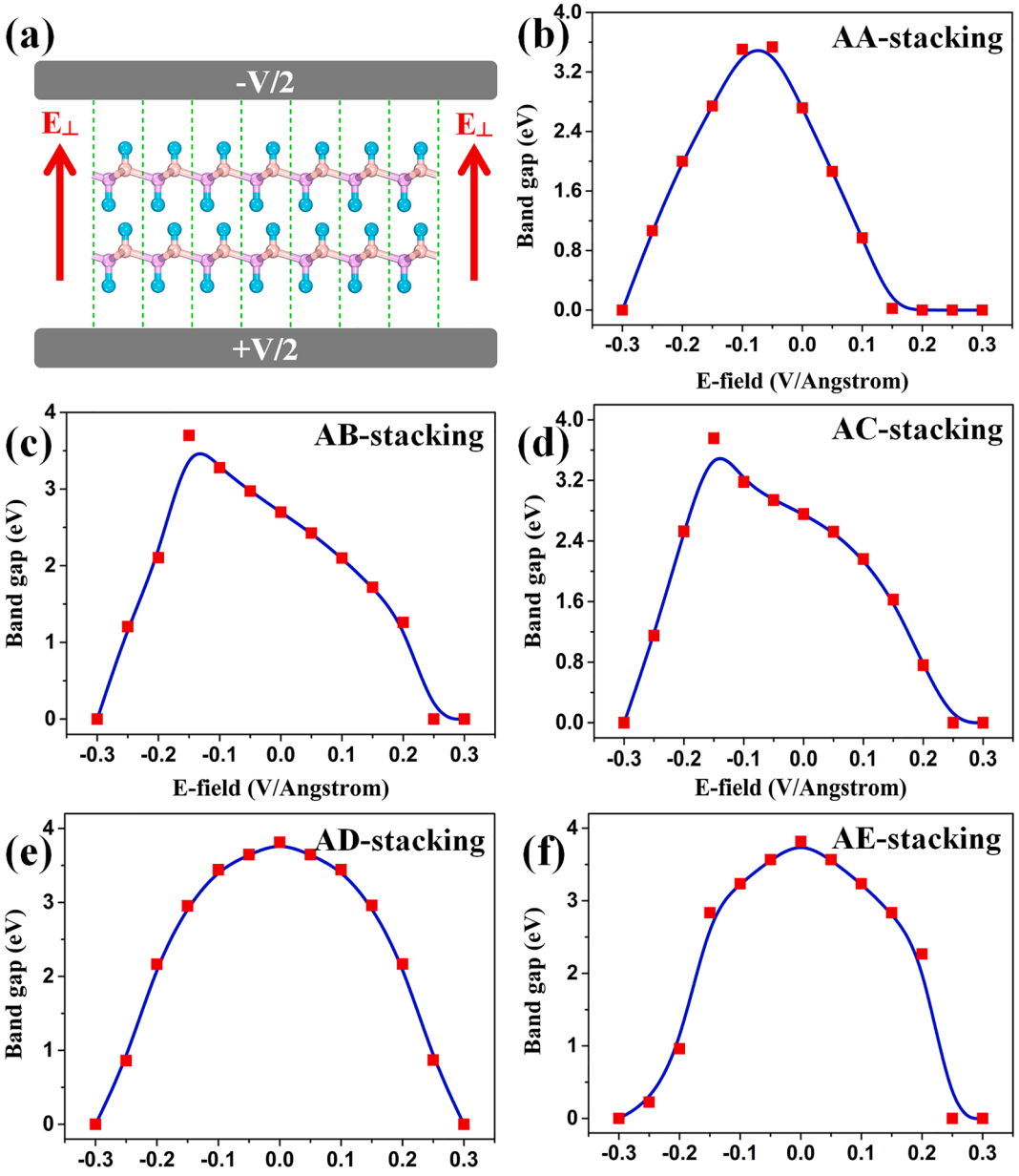

Fig. 5. (a) Schematic illustration of applied E-field in the bilayer hydrogenated BP, where the positive orientation of E-field is donated by red arrows. Vertical E-field dependent bandgap of (b) AA-, (c) AB-, (d) AC-, (e) AD-, and (f) AE-stacked bilayer hydrogenated BP.

electronic states of top and bottom layers, showing the π bond characteristic, which provides an indirect evidence for the effect of interlayer interaction on the band structure.[51,52] In the AD- and AE-stacked configurations, the electronic states of CBM and VBM are all localized on the both top and bottom layers, which is responsible for the slight increase of band gap.

A tremendous amount of theoretical and experimental achievements has shown that mechanical strain and external electrical field (E-field) can be a routine technique roadmap in effectively modulating the band structure, optical and magnetic properties, and interfacial barrier height at 2D materials based nanoelectronic devices.[53–57] As a result, it is an interesting investigation to explore the tunability of the electronic properties of different stacked patterns through mechanical strain and external E-field. In this section, the response of the electronic properties of five stacked configurations to external strain and E-field is primarily discussed.

As above discussed, the band gaps of AA-, AB-, and AC-stacked structures have a remarkable decrease compared to that of hydrogenated BP monolayer, whereas AD- and AE-stacked structures show a slight increase behavior. The underlying mechanism of these behaviors can be contributed to the splitting and degeneracy of conduction bands and valence bands that are induced by the interlayer interaction. Previous studies have found a giant Stark effect in few-layer C_2N[50], BN nanostructures[58], and MoS_2 bilayer[59], etc. This effect is responsible for the tunable of electronic structures of 2D materials under external E-field conditions. For the external strain, the tunable mechanism in the electronic structures is contributed from the high sensitivity of the band structures near the Fermi level to the orbital coupling/interaction-neighboring atoms within the crystal, and the magnitudes of external strain have a remarkable influence on the degree of orbitals interaction.[60] In order to clarify the tunable possibilities of perpendicular E-field and external strain in the electronic structures, the response of band structures of five stacked patterns to different E-field and mechanical strain are investigated. As shown in Fig. 5(a), the positive orientation of vertical E-field is taken as from bottom layer to top layer of bilayer hydrogenated BP. Clearly, the bandgap of five stacked

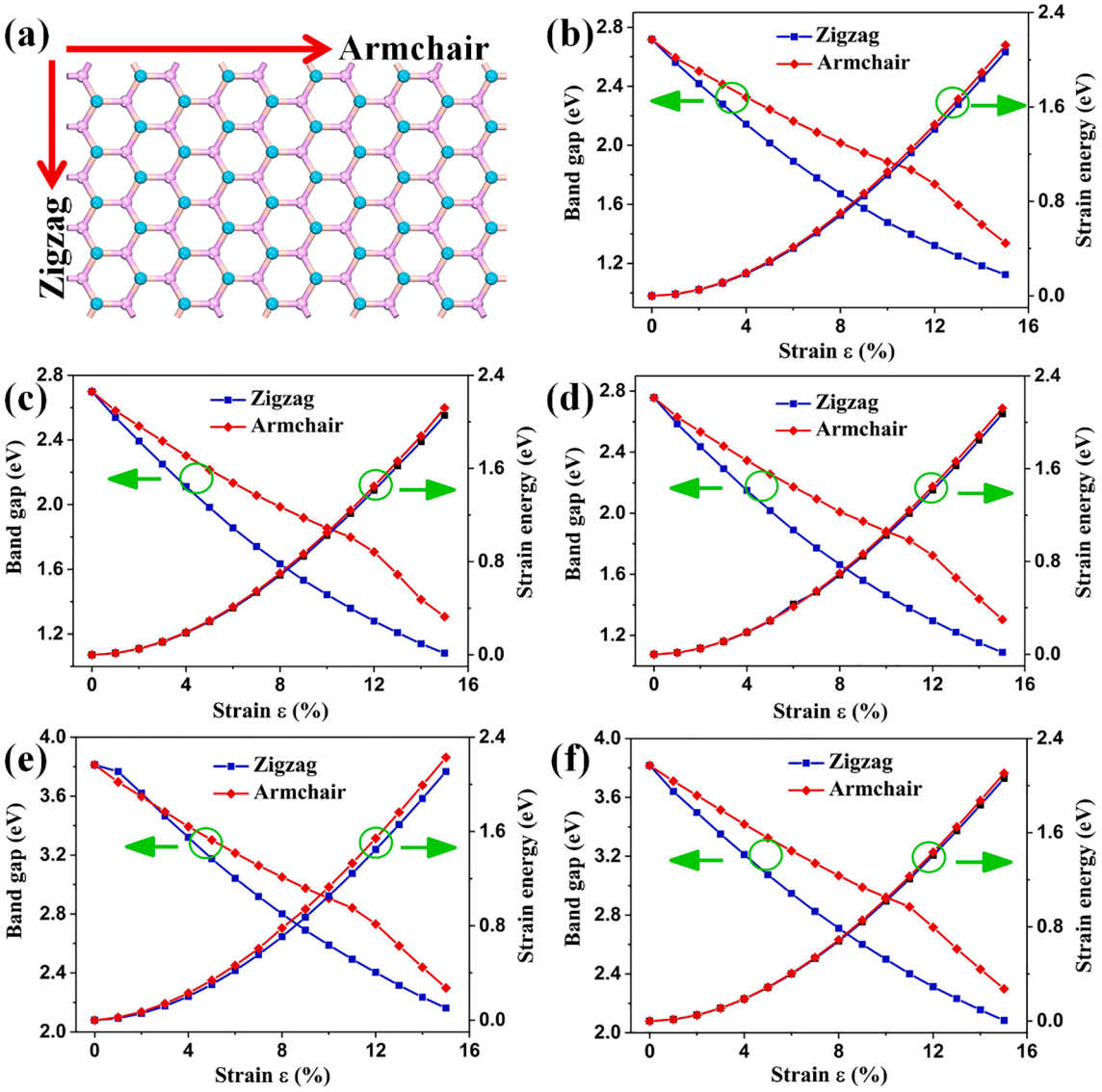

Fig. 6. The electronic properties of five stacked configurations varied with tensile strain. (a) Two directions of tensile strain applied in the different stacking orders. The variation of bandgap and strain energy of (b) AA-, (c) AB-, (d) AC-, (e) AD-, and (f) AE-stacked conformations as a function of tensile strain in the armchair and zigzag directions.

configurations is highly sensitive to the vertical E-field and the semiconductor–metal transition is observed at a sufficient E-field. For the AA-stacking, we find that the response of bandgap to vertical E-field within the range of −0.30 to 0.15 V/Å is a quasi-parabolic function in which the bandgaps decrease monotonously with the increase of the positive E-field, whereas for the negative E-field the bandgap firstly increases and then decreases in the investigated range. The non-symmetric variation of the bandgaps is attributed to the polarity of B and P atoms.[61,62] Notably, when the positive and negative E-fields are increased to 0.20 and −0.30 V/Å. respectively, the band structures of the AA-stacked pattern are transited to metallic feature from semiconductor characteristic. In Fig. 5(c) and (d), it is found that the variation trend of the bandgap of the AB-stacked configuration is almost similar to that of the AC-stacking, and the relationship between bandgap and E-field behaves a pseudo-shark fin shape. One can see that the bandgap of both two stacked patterns non-linearly decreases within the range from 0 to 0.30 V/Å, while in the range of −0.15 ~ 0.00 V/Å the bandgap shows a monotonic increasing trend. Interestingly, the bandgap is dramatically reduced when the negative E-field is increased in increments of −0.05 V/Å under the range of −0.30 ~ −0.15 V/Å, which indicates that a small external stimulus can be proposed as an effective tailoring tool in the electronic structures of advanced nanomaterials. For the AD- and AE-stacked configurations, the bandgap as a function of applied E-field exhibit a quasi-parabolic behavior and the bandgap non-linearly decreases with the increase of positive or negative E-field, as illustrated in Fig. 5(e) and (f). The distinguish between these two stacked patterns is that the bandgap variation of AD-stacking possesses the better parabolic curve, whereas it is not expected to obtain in the AE-stacked structure. When the negative E-field is set as −0.30 V/Å, the semiconductor–metal transition can be observed. For the positive E-field, the metallic feature of AD- and AE-stacking occurs at 0.30 and 0.25 V/Å, respectively.

In addition to the external E-field, the effect of mechanical strain (tensile strain) on the band structures of bilayer hydrogenated BP is also evaluated. Moreover, the strain energy is also taken into account to investigate the degree of structural deformation, being defined as $\Delta E = E_{deformed} - E_{pristine}$ in which $E_{deformed}$ and $E_{pristine}$ are the total energy of deformed and pristine stacked structure, respectively. As depicted in Fig. 6(a), there are two directions of tensile strain, namely armchair and zigzag orientations. The investigated range of tensile strain in the both

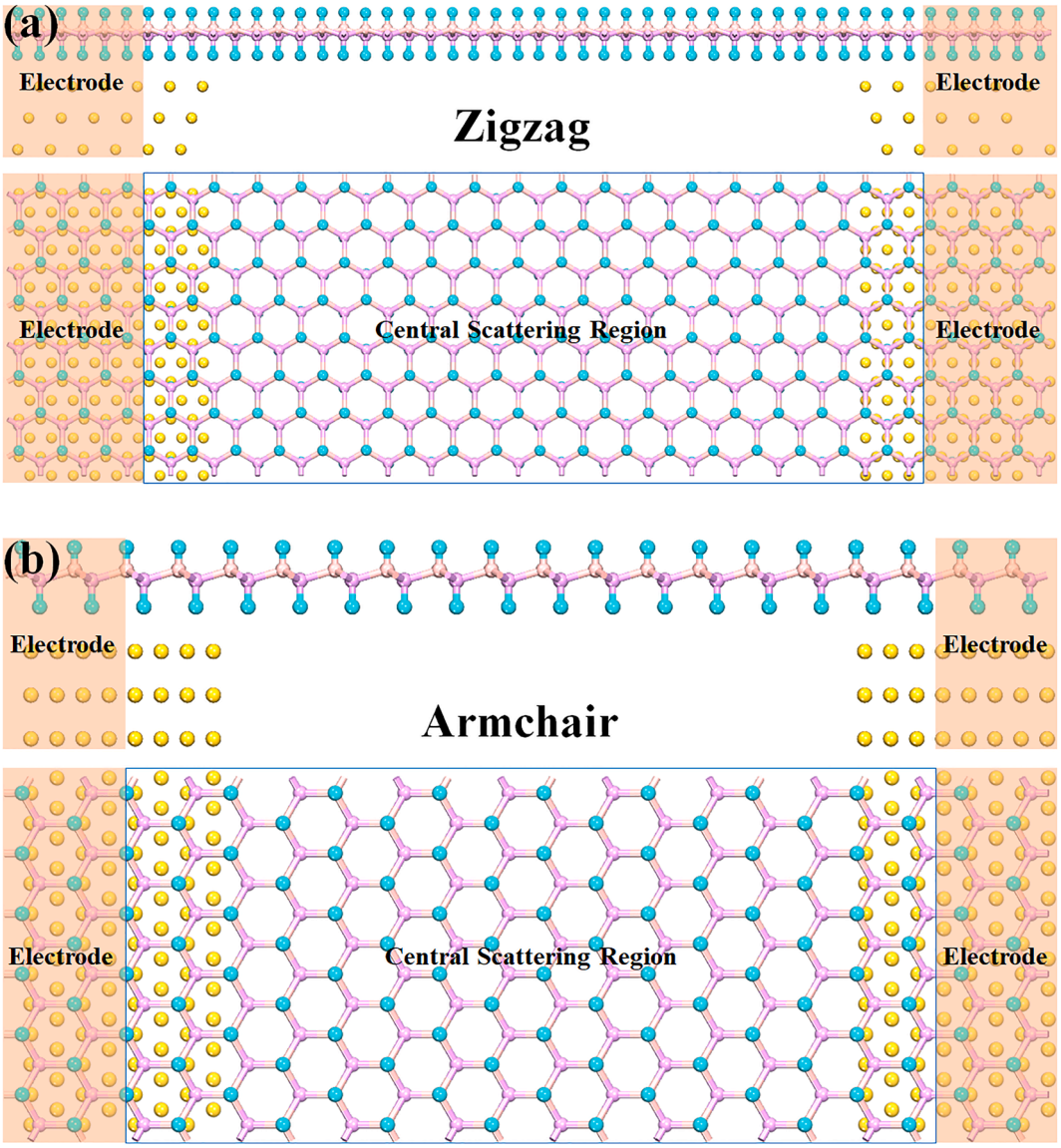

Fig. 7. Schematic representation of the two-probe configurations where metallic atoms (orange shade region) are acted as the semi-infinite left and right electrodes that are in contact with the central scattering region along the zigzag and armchair orientations.

orientations is selected from 0% to 15% to explore the limitation of the elastic deformation of various stacked conformations. For the tensile strain of zigzag direction, it can be distinctly observed that the bandgap of five stacked configurations displays a smooth nonlinear dependence with tensile strain, as plotted in Fig. 6(b)-(f). The bandgap monotonously decreases with the increasing of tensile strain under the investigated window of 0% to 15%. In the meantime, the corresponding bandgaps of AA-, AB-, AC-, AD-, and AE-stacked patterns are reduced by 1.59, 1.62, 1.67, 1.65, and 1.73 eV respectively after applying 15% of tensile strain. Compared to the case of the zigzag direction, the variation level of bandgap value for all stacking orders is smaller within the range of 0%–11% of tensile strain along the armchair orientation. Unexpectedly, the bandgap at 12%-15% tensile strain diverges from the decreasing principle observed at 0%-11%, and its reduction trend is steeper than that under other strain conditions. When the tensile strain is changed from 0% to 15%, the reduced bandgap values are 1.38, 1.39, 1.45, 1.51, and 1.52 eV for AA-, AB-, AC-, AD-, and AE-stacked structures, respectively. These values are smaller than that calculated in the zigzag orientation, which reveals that the bandgap variation is dependent of the strain direction to a certain extent. In addition, the strain energy at the corresponding tensile strain is also computed to provide a quantitative description for evaluating the limitation of elastic deformation of various stacked configurations. The dependence of the bandgap on tensile strain for different stacking orders is presented in Fig. 6(b)-(f). As we can see, the strain energies for all the investigated stacking orders monotonously increase with a smooth curve at 0%-15% tensile strain along zigzag or armchair direction. The range of elastic deformation of bilayer hydrogenated BP is comparable to that of ultrathin black phosphorus, and larger than the AlAs/germanene heterostructure.[23,55] Besides, there is not a positive to negative transition in the strain energy for both zigzag and armchair orientations. These results confirm that the 0%-15% tensile strain belongs to the scope of elastic deformation where the deformation structure induced by the external strain can be restored to the original state after removing the tensile strain. At the same time, the strain energies in both zigzag and armchair orientations are almost the same, suggesting that the strain energies are independent of the stacking orders and the orientation of tensile strain. Unfortunately, as shown in Figure S6, there are imaginary frequency in the AA structures when the tensile strength is applied from 11% to 15% in the armchair direction. Therefore, it can get a conclusion that the elastic deformation capacity of HBP bilayers is much weaker than that of graphene.

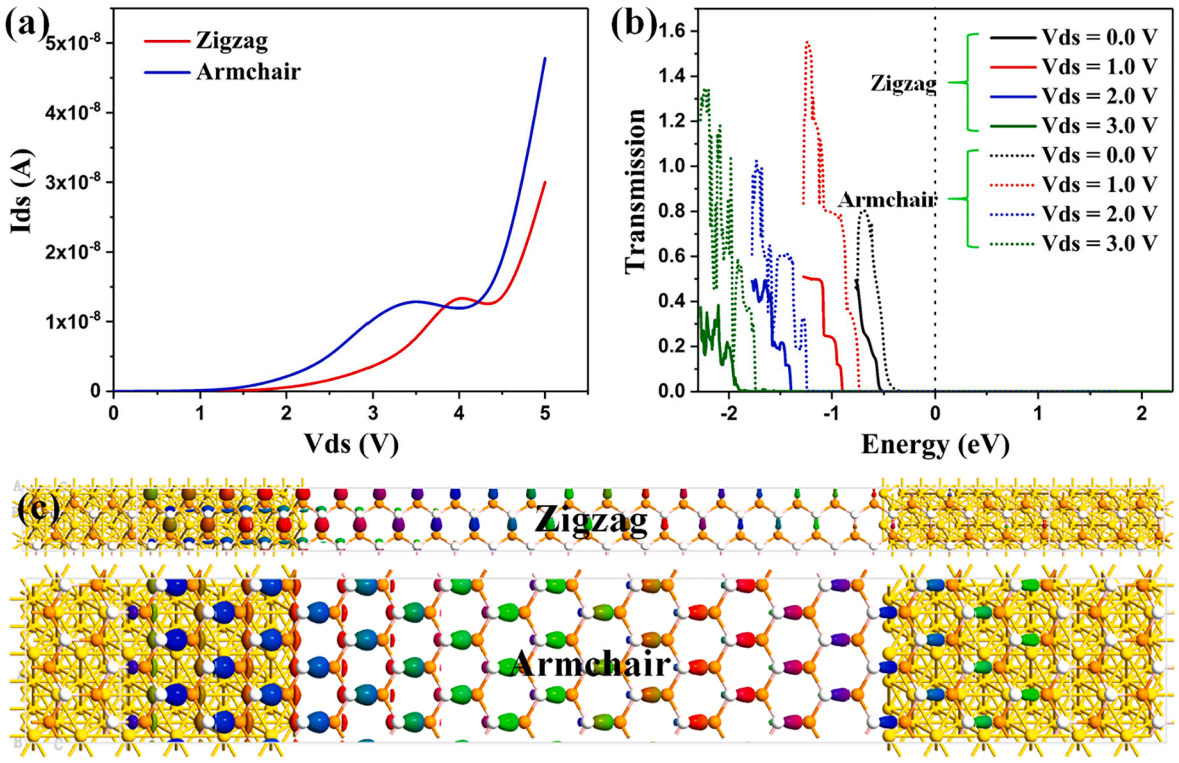

Fig. 8. (a) The I-V characterization and (b) Bias-dependent transmission spectrum of hydrogenated BP monolayer along zigzag and armchair orientations. Isosurface plots of the computed zigzag and armchair directional transmission eigenstates at an energy of −1.0 eV under a bias of 3.0 V are presented in (c). The Fermi level is set to zero.

As the above discussed, bilayer hydrogenated BP constructed by different stacking orders possesses the outstanding tunability in the electronic structures by mean of external stimulus (i.e. mechanical strain and E-field). However, it cannot be directly confirmed that hydrogenated BP layer has remarkable electronic performance in the device level. Consequently, to definitely estimate the performance of hydrogenated BP layer as a nanoelectronic device, we perform the calculations of transport transmission and current–voltage (I-V) characteristic by employing the non-equilibrium Green's function (NEGF) approach. The NEGF method has broken through the barrier between the experimental and theoretical researches, and the results based on this method can be directly compared with the data measured in the experiment. Previous studies have clearly shown that the electron transport is dependent on the structural anisotropy, thus two transport models along zigzag and armchair directions are constructed in the transport calculations. [30,63–65] Two representative configurations of the two-probe systems consisted of hydrogenated BP monolayer along zigzag and armchair orientations are illustrated in Fig. 7. For the zigzag case, the central scattering region is constructed by a 1×12 supercell, whereas a 3×12 supercell is considered in the armchair case. In addition, the lattice-constant mismatching of hydrogenated BP monolayer with Au layer is negligible because the mismatch is less than 2% in the zigzag and armchair orientations. The calculated I-V curves along the zigzag and armchair orientations of hydrogenated BP monolayer is shown in Fig. 8 (a). The current passing through the central scattering region can be approximately zero before the bias between left and right electrodes is up to 1.5 V. The inherent mechanism is attributed to the location shifting of the Fermi level of the left electrode of the two-probe configuration with respect to the right electrode. When the VBM of the left electrode touches the CBM of the right electrode, the current begins to gradually increase from zero. As a result, with the further increasing of the bias voltage between two electrodes, the currents along the zigzag and armchair directions increase rapidly. This is the expected characteristics in the wide-bandgap semiconductors. Unsurprisingly, the total current passing the hydrogenated BP monolayer is only of the order of nano-Amperes (nA) regardless of the transport direction, which is several orders of magnitude smaller than that flowing through phosphorene nanoribbon along the armchair orientation under the same bias voltage. [66] Besides, it can be noted that the currents of the armchair directional configuration are significantly larger than that along the zigzag orientation, which reveals that hydrogenated BP monolayer possesses the feature of transport anisotropy. Interestingly, a negative differential resistive (NDR) behavior is clearly observed in the computed I-V characteristics, suggesting that hydrogenated BP monolayer has a promising application prospect in the field of high-frequency oscillators and field-effect transistors.[67,68] As the increase of the bias voltage within the range of 3.5 to 4.0 V (armchair direction) and 4.0 to 4.5 V (zigzag direction), the total current of the two-probe devices has a slight reduction behavior. In comparison to the phosphorene nanoribbon with the zigzag direction, the NDR effect in hydrogenated BP monolayer is less prominent, whereas it is equivalent to that of the armchair silicene nanoribbons in variation level.[66,69] Furthermore, the transmission spectrums of the two-probe configurations constructed by hydrogenated BP monolayer under various applied biases are calculated to better understand the I-V characteristics of hydrogenated BP. In Fig. 8(b), we find that the transmission coefficient of the armchair directional configuration is higher than that along the zigzag direction at the same applied bias. This result further confirms the transmission anisotropy of hydrogenated BP. Meanwhile, the potential barriers for holes (Φ_h) in both two orientations are dependence with the biases applied to the left and right electrodes. As we can see, the Φ_h increases with the increasing of the applied bias and the corresponding values for the zigzag configuration are larger than that along the armchair direction. For the two-/three-terminal devices, the current path in channel materials is a critical technique point. Therefore, in order to distinctly trace the transmission pathway for electrons or holes, we perform the calculations of transmission eigenstates. Fig. 8(c) presents the isosurface plots of the computed zigzag and armchair directional transmission eigenstates at

an energy of −1.0 eV under a bias of 3.0 V. One can see that the amplitude of the eigenstates gradually decreases along the transmission direction and the eigenstates on the right side of the central scattering region can be clearly observed. It reflects that the incident states on the left side of the central scattering region have the large transmission probability to pass through the scattering region and reach the right electrode. Nevertheless, the amplitude of the eigenstates for the armchair orientation is larger than that along the zigzag orientation, which further confirms that the armchair configuration possesses a higher transmission coefficient.

4. Conclusions

In summary, we systematically describe the structural, electronic, and transport properties of hydrogenated BP layer by means of the first principles calculations. The effect of stacking orders and external stimulus (i.e. mechanical strain and external E-field) on the electronic structures is also investigated. Our results show that BP monolayer passivated by hydrogenation possesses the buckled honeycomb structure with an indirect gap of 3.76 eV and the binding of the AA-, AB-, and AE-stacked patterns is the strongest among five the stacked configurations. In comparison to the bandgap of the hydrogenated BP monolayer, the bandgaps in AA- and AB-stacking are induced by 1.0 eV, whereas for AE-stacking the band structure is slightly enlarged. This behavior is ascribed to the splitting and degeneracy of conduction bands and valence bands. For the external E-field, the bandgap of five stacked configurations is highly sensitive to the vertical E-field and the semiconductor–metal transition is observed at a sufficient E-field. In the strain calculations, we find that the bandgap decreases monotonously with the increasing of the tensile strain within the range of 0–15% and the positive to negative transition in the strain energies is not observed in the investigated range regardless of the strain direction. These results suggest that the mechanical strain and E-field can effectively modulate the electronic properties, being expected in the device applications. Transport calculations present the existence of the transmission anisotropy and the negative differential resistive behavior, indicating that hydrogenated BP holds the promising potential for the field of high-frequency oscillators and field-effect transistors. At the same bias, the total current flowing through the hydrogenated BP is several orders of magnitude smaller than that in graphene-like materials. These outstanding properties present prospective applications of nanoelectronics and micro-power devices based on hydrogenated BP.

CRediT authorship contribution statement

Chunjian Tan: Formal analysis, Investigation, Writing – original draft. **Quan Zhou:** Investigation, Visualization. **Xu Liu:** Data curation, Visualization. **Guoqi Zhang:** Project administration, Funding acquisition. **Huaiyu Ye:** Writing – review & editing, Supervision. **Qibao Wu:** Funding acquisition.

Declaration of Competing Interest

The authors declare that they have no known competing financial interests or personal relationships that could have appeared to influence the work reported in this paper.

Acknowledgement

This work was supported by the National Key R&D Program of China (2018YFE0204600), the Key-Area Research and Development Program of GuangDong Province (2019B010131001), the Shenzhen Science and Technology Plan Project (GJHZ20180929154602092), and the Shenzhen Fundamental Research Program (JCYJ20200109140822796).

References

[1] S.B. Desai, S.R. Madhvapathy, A.B. Sachid, J.P. Llinas, Q. Wang, G.H. Ahn, G. Pitner, M.J. Kim, J. Bokor, C. Hu, MoS2 transistors with 1-nanometer gate lengths, Science 354 (2016) 99–102.
[2] Y. Li, S. Yang, J. Li, Modulation of the electronic properties of ultrathin black phosphorus by strain and electrical field, J. Phys. Chem. C 118 (2014) 23970–23976.
[3] D. Hisamoto, W.-C. Lee, J. Kedzierski, H. Takeuchi, K. Asano, C. Kuo, E. Anderson, T.-J. King, J. Bokor, C. Hu, FinFET-a self-aligned double-gate MOSFET scalable to 20 nm, IEEE Trans. Electron Devices 47 (2000) 2320–2325.
[4] B. Yu, L. Chang, S. Ahmed, H. Wang, S. Bell, C.-Y. Yang, C. Tabery, C. Ho, Q. Xiang, T.-J. King, FinFET scaling to 10 nm gate length, in: Electron Devices Meeting, 2002. IEDM'02. International, IEEE, 2002, pp. 251-254.
[5] S. Gupta, V. Moroz, L. Smith, Q. Lu, K.C. Saraswat, 7-nm FinFET CMOS design enabled by stress engineering using Si Ge, and Sn, IEEE Transactions on Electron Devices 61 (2014) 1222–1230.
[6] A.D. Franklin, Nanomaterials in transistors: From high-performance to thin-film applications, Science 349 (2015), aab2750.
[7] H. Jeong, S. Bang, H.M. Oh, H.J. Jeong, S.J. An, G.H. Han, H. Kim, K.K. Kim, J. C. Park, Y.H. Lee, Semiconductor-Insulator-Semiconductor Diode Consisting of Monolayer MoS2, h-BN, and GaN Heterostructure, ACS Nano 9 (2015) 10032–10038.
[8] J.D. Li, J.J. Cheng, B. Miao, X.W. Wei, J. Xie, J.C. Zhang, Z.Q. Zhang, D.M. Wu, Detection of prostate-specific antigen with biomolecule-gated AlGaN/GaN high electron mobility transistors, J. Micromech. Microeng. 24 (2014), 075023.
[9] C.E. Dreyer, A. Janotti, d.W. Van, Effects of strain on the electron effective mass in GaN and AlN, Appl. Phys. Lett. 102 (2013) 142105.
[10] M. Xie, S. Zhang, B. Cai, Z. Zhu, Y. Zou, H. Zeng, Two-dimensional BX (X = P, As, Sb) semiconductors with mobilities approaching graphene, Nanoscale 8 (2016).
[11] H.L. Zhuang, R.G. Hennig, Electronic Structures of Single-Layer Boron Pnictides, Appl. Phys. Lett. 101 (2012), 153109.
[12] X. Chen, C. Tan, Q. Yang, R. Meng, Q. Liang, J. Jiang, X. Sun, D.Q. Yang, T. Ren, Effect of multilayer structure, stacking order and external electric field on the electrical properties of few-layer boron-phosphide, PCCP 18 (2016).
[13] S. Dalui, A.K. Pal, Synthesis of n-type boron phosphide films and formation of Schottky diode: Al/n-BP/Sb, Appl. Surf. Sci. 254 (2008) 3540–3547.
[14] D. Kecik, H. Sahin, E. Durgun, F.M. Peeters, Realization of a p-n junction in a single layer boron-phosphide, PCCP 17 (2015) 13013–13020.
[15] J.I. Ejembi, I.H. Nwigboji, L. Franklin, Y. Malozovsky, Ab-initio calculations of electronic, transport, and structural properties of boron phosphide, J. Appl. Phys. 116 (2014), 103711.
[16] M.M. Obeid, H.R. Jappor, K. Al-Marzoki, D. Hoat, T.V. Vu, S.J. Edrees, Z.M. Yaseen, M.M.J.C.M.S. Shukur, Electronic and magnetic properties of single-layer boron phosphide associated with materials processing defects, 170 (2019), 109201.
[17] J. Yu, W.J.A.P.L. Guo, Strain tunable electronic and magnetic properties of pristine and semihydrogenated hexagonal boron phosphide, 106 (2015), 043107.
[18] M.Q. Long, L. Tang, D. Wang, L. Wang, Z. Shuai, Theoretical predictions of size-dependent carrier mobility and polarity in graphene, J. Am. Chem. Soc. 131 (2009) 17728–17729.
[19] S. Bruzzone, G. Fiori, Ab-Initio Simulations of Deformation Potentials and Electron Mobility in Chemically Modified Graphene and two-dimensional hexagonal Boron-Nitride, Appl. Phys. Lett. 99 (2011) 610.
[20] J. Qiao, X. Kong, Z.X. Hu, F. Yang, W. Ji, High-mobility transport anisotropy and linear dichroism in few-layer black phosphorus, Nat. Commun. 5 (2014) 4475.
[21] K. Takahashi, A. Yoshikawa, A. Sandhu, Wide bandgap semiconductors, Springer, 2007.
[22] M.-J. Sun, X. Cao, Z. Cao, Si (C□ C) 4-Based Single-Crystalline Semiconductor: Diamond-like Superlight and Superflexible Wide-Bandgap Material for the UV Photoconductive Device, ACS Appl. Mater. Interfaces 8 (2016) 16551–16554.
[23] C. Tan, Q. Yang, R. Meng, Q. Liang, J. Jiang, X. Sun, H. Ye, X. Chen, An AlAs/germanene heterostructure with tunable electronic and optical properties via external electric field and strain, J. Mater. Chem. C 4 (2016) 8171–8178.
[24] X. Chen, J. Jiang, Q. Liang, R. Meng, C. Tan, Q. Yang, S. Zhang, H. Zeng, Tunable electronic structure and enhanced optical properties in quasi-metallic hydrogenated/fluorinated SiC heterobilayer, J. Mater. Chem. C 4 (2016) 7406–7414.
[25] J. Jiang, Q. Liang, S. Zhang, R. Meng, C. Tan, Q. Yang, X. Sun, H. Ye, X. Chen, Tuning the electronic and optical properties of graphane/silicane and fhBN/silicane nanosheets via interfacial dihydrogen bonding and electrical field control, J. Mater. Chem. C 4 (2016) 8962–8972.
[26] S. Trivedi, A. Srivastava, R. Kurchania, Silicene and germanene: a first principle study of electronic structure and effect of hydrogenation-passivation, J. Comput. Theor. Nanosci. 11 (2014) 781–788.
[27] V. Zolyomi, J. Wallbank, V. Fal'Ko, Silicane and germanane: tight-binding and first-principles studies, 2D Materials 1 (2014), 011005.
[28] C. Zhou, S. Chen, J. Lou, J. Wang, Q. Yang, C. Liu, D. Huang, T. Zhu, Graphene's cousin: the present and future of graphane, Nanoscale Res. Lett. 9 (2014) 26.
[29] L. Huang, Y. Li, Z. Wei, J. Li, Strain induced piezoelectric effect in black phosphorus and MoS2 van der Waals heterostructure, Sci. Rep. 5 (2015).
[30] Y. Xu, J. Dai, X.C. Zeng, Electron-Transport Properties of Few-Layer Black Phosphorus, J. Phys. Chem. Lett. 6 (2015) 1996.
[31] C. Wu, H. Wang, J. Zhang, G. Gou, B. Pan, J. Li, Lithium-Boron (Li–B) Monolayers: First-Principles Cluster Expansion and Possible Two-Dimensional Superconductivity, ACS Appl. Mater. Interfaces 8 (2016).

[32] K. Ma, H. Wang, J. Wang, Q. Wang, Strain-engineering of bandgaps in pristine and fully hydrogenated hexagonal boron phosphide, J. Appl. Phys. 128 (2020), 094302.
[33] Y.P. Wang, W.X. Ji, C.W. Zhang, P. Li, F. Li, M.J. Ren, X.L. Chen, M. Yuan, P. J. Wang, Controllable band structure and topological phase transition in two-dimensional hydrogenated arsenene, Sci. Rep. 6 (2016) 20342.
[34] J. Yun, G. Lee, K.S. Kim, Electron Transport in Graphene Nanoribbon Field-Effect Transistor under Bias and Gate Voltages: Isochemical Potential Approach, J. Phys. Chem. Lett. 7 (2016) 2478.
[35] E. Cadelano, P.L. Palla, S. Giordano, L. Colombo, Elastic properties of hydrogenated graphene, Phys. Rev. B 82 (2010), 235414.
[36] L.-F. Huang, P.-L. Gong, Z. Zeng, Phonon properties, thermal expansion, and thermomechanics of silicene and germanene, Phys. Rev. B 91 (2015), 205433.
[37] Y.-P. Wang, W.-X. Ji, C.-W. Zhang, P. Li, F. Li, M.-J. Ren, X.-L. Chen, M. Yuan, P.-J. Wang, Controllable band structure and topological phase transition in two-dimensional hydrogenated arsenene, Sci. Rep. 6 (2016).
[38] R. Thapa, G. Das, Optical and vibrational properties of hydrogenated BN-sheet: First principles study, Appl. Surf. Sci. 284 (2013) 638–643.
[39] S. Zhang, Y. Hu, Z. Hu, B. Cai, H. Zeng, Hydrogenated arsenenes as planar magnet and Dirac material, Appl. Phys. Lett. 107 (2015), 022102.
[40] L. Li, Z. Chen, Y. Hu, X. Wang, T. Zhang, W. Chen, Q. Wang, Single-layer single-crystalline SnSe nanosheets, J. Am. Chem. Soc. 135 (2013) 1213–1216.
[41] M. Buscema, D.J. Groenendijk, G.A. Steele, H.S. Van Der Zant, A. Castellanos-Gomez, Photovoltaic effect in few-layer black phosphorus PN junctions defined by local electrostatic gating, Nat. Commun. 5 (2014) 1–6.
[42] A. Bhattacharya, S. Bhattacharya, G. Das, Strain-induced band-gap deformation of H/F passivated graphene and h-BN sheet, Phys. Rev. B 84 (2011), 075454.
[43] M. Sun, S. Wang, J. Yu, W. Tang, Hydrogenated and halogenated blue phosphorene as Dirac materials: A first principles study, Appl. Surf. Sci. 392 (2017) 46–50.
[44] A. Bhattacharya, S. Bhattacharya, G. Das, Band gap engineering by functionalization of BN sheet, Phys. Rev. B 85 (2012), 035415.
[45] S. Ullah, P.A. Denis, F.J.A.o. Sato, Hydrogenation and fluorination of 2D boron phosphide and boron arsenide: a density functional theory investigation, 3 (2018), 16416-16423.
[46] X. Peng, Q. Wei, A.J.P.R.B. Copple, Strain-engineered direct-indirect band gap transition and its mechanism in two-dimensional phosphorene 90 (2014), 085402.
[47] O.M. Hernández, J. Guerrero-Sánchez, R. Ponce-Pérez, R.G. Díaz, H. Fernandez-Escamilla, G.H.J.A.S.S. Cocoletzi, Hexagonal boron phosphide monolayer exfoliation induced by arsenic incorporation in the BP (1 1 1) surface: A DFT study, 538 (2021), 148163.
[48] W. Zhang, Q. Wang, Y. Chen, Z. Wang, A.T. Wee, Van der Waals stacked 2D layered materials for optoelectronics, 2D Materials 3 (2016), 022001.
[49] J. Dai, X.C. Zeng, Bilayer phosphorene: effect of stacking order on bandgap and its potential applications in thin-film solar cells, J. Phys. Chem. Lett. 5 (2014) 1289–1293.
[50] R. Zhang, B. Li, J. Yang, Effects of stacking order, layer number and external electric field on electronic structures of few-layer C 2 N-h 2D, Nanoscale 7 (2015) 14062–14070.
[51] X. Chen, R. Meng, J. Jiang, Q. Liang, Q. Yang, C. Tan, X. Sun, S. Zhang, T. Ren, Electronic structure and optical properties of graphene/stanene heterobilayer, PCCP 18 (2016) 16302–16309.
[52] Q. Zheng, G. Luo, Q. Liu, R. Quhe, J. Zheng, K. Tang, Z. Gao, S. Nagase, J. Lu, Structural and electronic properties of bilayer and trilayer graphdiyne, Nanoscale 4 (2012) 3990–3996.
[53] C. Tan, Q. Yang, R. Meng, Q. Liang, J. Jiang, X. Sun, H. Ye, X.J.J.o.M.C.C. Chen, An AlAs/germanene heterostructure with tunable electronic and optical properties via external electric field and strain, 4 (2016), 8171-8178.
[54] Z. Dai, L. Liu, Z. Zhang, Strain engineering of 2D materials: issues and opportunities at the interface, Adv. Mater. 31 (2019) 1805417.
[55] Y. Li, S. Yang, J.J.T.J.o.P.C.C. Li, Modulation of the electronic properties of ultrathin black phosphorus by strain and electrical field, 118 (2014), 23970-23976.
[56] D. Chen, X. Lei, Y. Wang, S. Zhong, G. Liu, B. Xu, C. Ouyang, Tunable electronic structures in BP/MoSSe van der Waals heterostructures by external electric field and strain, Appl. Surf. Sci. 497 (2019), 143809.
[57] Z. Xie, F. Sun, R. Yao, Y. Zhang, Y. Zhang, Z. Zhang, J. Fan, L. Ni, L. Duan, Tuning electronic properties of InSe/arsenene heterostructure by external electric field and uniaxial strain, Appl. Surf. Sci. 475 (2019) 839–846.
[58] A. Aldalbahi, A.F. Zhou, P. Feng, Variations in Crystalline Structures and Electrical Properties of Single Crystalline Boron Nitride Nanosheets, Sci. Rep. 5 (2015) 16703.
[59] J. Klein, J. Wierzbowski, A. Regler, J. Becker, F. Heimbach, K. Müller, M. Kaniber, J.J. Finley, Stark Effect Spectroscopy of Mono- and Few-Layer MoS2, Nano Lett. (2016).
[60] S. Yang, C. Wang, H. Sahin, H. Chen, Y. Li, S.S. Li, A. Suslu, F.M. Peeters, Q. Liu, J. Li, Tuning the Optical, Magnetic, and Electrical Properties of ReSe ₂ by Nanoscale Strain Engineering, Nano Lett. 15 (2015) 1660–1666.
[61] J. Wang, P. Zhang, X.-M.J.C.P.B. Duan, First-principles modeling hydrogenation of bilayered boron nitride 25 (2016), 057301.
[62] D.K. Samarakoon, X.-Q.J.A.n. Wang, Tunable band gap in hydrogenated bilayer graphene, 4 (2010), 4126-4130.
[63] L. Kou, T. Frauenheim, C. Chen, Phosphorene as a superior gas sensor: selective adsorption and distinct I-V response, J. Phys. Chem. Lett. 5 (2014) 2675–2681.
[64] A. Naeemi, J.D. Meindl, Electron transport modeling for junctions of zigzag and armchair graphene nanoribbons (GNRs), IEEE Electron Device Lett. 29 (2008) 497–499.
[65] A. Orlof, J. Ruseckas, I.V. Zozoulenko, Effect of zigzag and armchair edges on the electronic transport in single-layer and bilayer graphene nanoribbons with defects, Phys. Rev. B 88 (2013) 4673–4677.
[66] A. Maity, A. Singh, P. Sen, A. Kibey, A. Kshirsagar, D.G. Kanhere, Structural, electronic, mechanical, and transport properties of phosphorene nanoribbons: Negative differential resistance behavior, Phys. Rev. B 94 (2016), 075422.
[67] Y. Wu, D.B. Farmer, W. Zhu, S.-J. Han, C.D. Dimitrakopoulos, A.A. Bol, P. Avouris, Y.-M. Lin, Three-terminal graphene negative differential resistance devices, ACS Nano 6 (2012) 2610–2616.
[68] J. Sakai, High-efficiency voltage oscillation in VO 2 planer-type junctions with infinite negative differential resistance, J. Appl. Phys. 103 (2008), 103708.
[69] S. Singh, A. De Sarkar, B. Singh, I. Kaur, Electronic and transport behavior of doped armchair silicene nanoribbons exhibiting negative differential resistance and its FET performance, RSC Adv. 7 (2017) 12783–12792.